Monitoring of Ageing Campaigns of PEM Fuel Cell Stacks Using a Model-Based Method

Sami El Aabid*‡, Christophe Turpin*, Jeremi Regnier*, Julien D'Arbigny**, Theophile Horde***, Alexandra Pessot*

* Department of electrical research, Laplace laboratory, University of Toulouse, CNRS, INPT, UPS, F-31071 Toulouse, France

** Safran Aerosystems, F-78373 Plaisir, France

*** Safran Power Units, F-31019 Toulouse

(elaabid@laplace.univ-tlse.fr, turpin@laplace.univ-tlse.fr, regnier@laplace.univ-tlse.fr, Julien.darbigny@safran.fr, theophile.horde@safran.fr, pessot@laplace.univ-tlse.fr)

‡ Corresponding Author; Sami El Aabid, Laplace laboratory, University of Toulouse, CNRS, INPT, UPS, F-31071 Toulouse, France, Tel: +33 641 862 102, elaabid@laplace.univ-tlse.fr

Received: 12.11.202 Accepted:18.01.2021

Abstract- Nowadays, Proton Exchange Membrane Fuel Cells (PEMFC) are considered as a promising solution for transportation applications, especially for the aeronautical field in the context of development of a "More Electrical Aircraft". Due to various operating conditions, the State of Health (SoH) of a Proton Exchange Membrane Fuel Cell (PEMFC) could be degraded implying a possible decrease of its performance and durability. Hence, there must be a development of tools dedicated to the PEMFC diagnosis and ageing monitoring. In this context, this paper introduces a model-based method contributing to the monitoring of the SoH of a PEMFC in aircraft applications. The proposed methodology consists of the tracking of the temporal evolution a chosen Quasi-Static (QS) model parameters, these parameters being associated with the various physicochemical phenomena involved in a Fuel Cell (FC): activation, diffusion and ohmic. Parameters of the model are identified from a measurement regularly carried out throughout the fuel cell life: the polarization curve (V–I curve). The present model uses also high-frequency resistance measured via Electrochemical Impedance Spectroscopies (EIS) performed at various current values of the polarization curve. This methodology is evaluated here in the framework of three ageing campaigns carried out with three 1 kW PEM stacks operating at low temperature (50 – 80 °C). In this paper, a particular attention is paid to calculations and results relating to the first ageing campaign. A comparison of the results related to the three campaigns is achieved as a part of this work. In addition to the good reproduction of experimental data and the separation of losses in the static domain, the QS model presented in this paper makes it possible to monitor the FC SoH via the follow-up of losses and their related parameters.

Keywords Proton Exchange Membrane Fuel Cell (PEMFC), stack, ageing, polarization curve (V–I curve), Electrochemical Impedance Spectroscopy (EIS), State of Health (SoH).

1. Introduction

The PEM fuel cell is an ecological device making it possible to generate electricity, heat and water by using hydrogen and oxygen (coming from air or pure). Thanks to its good efficiency and high energy density, the PEMFC is considered as a good candidate for energy storage and/ or production.

FCs are submitted to ageing and various operating conditions leading to several failures such as hydrogen crossover [1] [2], electrode degradations [2] [3] or abnormal operation modes (flooding or drying). The understanding of ageing mechanisms of the PEMFC remain to be enhanced particularly on the aeronautical field [4] [5] where expectations in terms of lifetime are higher than those of electric vehicle applications [6] [7] [8] [9] for instance. Therefore, methods dedicated to the SoH monitoring and diagnosis of the FC have to be developed. Several tools are proposed in the literature concerning the ageing and the diagnosis of failures in FCs [10] [11] [12]. Reviews of different diagnosis tools can be found in [13] [14].

One of reliable approaches used for the FC SoH monitoring is based on parametric identification of a model through experimental data [15] [16] [17]. Widely used for the FC characterization, the V-I curve and the EIS coupled with a model describing the involved phenomena may provide further information about the FC SoH.

On the one hand, the V-I curve is generally used to study the impact of operational conditions [18], or the evolution of intrinsic FC parameters as a function of operational conditions [19] [20] [21]. On the other hand, the EIS makes it possible to carry out several studies such as hydric conditions assessment (flooding or drying) [22] [23] [24] [25], tracking of the internal resistance [26] [27], detection of hydrogen crossover [28] [29] or the evaluation of a stack performances [30]. More recent articles present a new approach consisting in the identification of generic models based on R-C cells in series through EIS measurements. These models allow to generate spectra of time-constants related to the dynamic involved phenomena, such as impedance spectra [15] [31]. A review of different diagnosis schemes based on EIS can be found in [32].

The contribution of our works is to conjointly exploit both characterizations: V-I curve and EIS. This exploitation is firstly achieved via the identification of two models, respectively for the QS (V–I curve) and the dynamic (EIS) domains. Secondly, the originality of this work is to ensure the consistency between both domains by introducing into each parametrization process, parameters and/or laws coming from the other part (see Fig.1) [15]. I.e., the ohmic resistance used in the QS model is stemming from the EIS and laws governing the dynamic model are derived from the QS model outputs.

The aim of the present article is in fine to separate and quantify each involved phenomenon with a robust and consistent model-based approach and to be able to monitor the FC ageing through the time evolution of each phenomenon and its related parameters.

Regarding the complexity of the developed dynamic model, we will just focus, in this article, on the framed part of the Fig.1. In other words, a quasi-static model will be identified from V-I data using the high-frequency resistance obtained via the EIS.

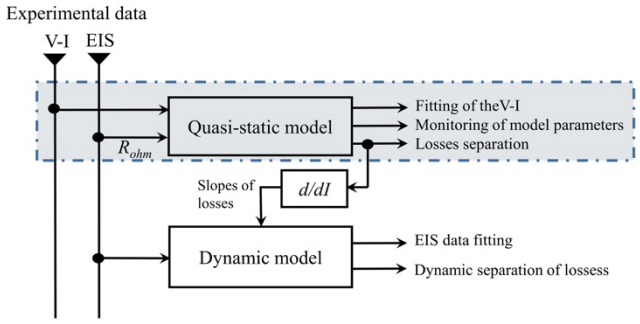

Fig. 1. Dedicated process to the identification of QS and dynamic models

In our previous works [15] were oriented towards the calibration of this approach using a cell with various sets of materials/ components to emulate various failures. These first encouraging works make it possible to consider the monitoring of the ageing of fuel cell stacks by the model-based methodology. In the present paper, the proposed method is applied to three ageing campaigns involving three 6-cell stacks (1 kW each operating under H_2/ Air) provided by Safran Aerosystems. The presented mission profiles in this paper correspond to an aeronautical application. Operating conditions are regarded constant during the mission profile.

2. Presentation of the model and experimental approach

2.1. Quasi-static model used

The Fuel Cell voltage V_{FC} can be expressed theoretically by the Equation (1) (valid for a single cell or the equivalent average cell of a stack):

$$V_{FC} = E_{th} - \eta_{ohm} - \eta_{act} - \eta_{diff} \quad (1)$$

where η_{ohm}, η_{act}, η_{diff} correspond respectively to the losses linked to the ohmic, chemical activation, and gas diffusion phenomena. E_{th} is the maximum theoretical voltage; it follows Nernst's law (see Equation (2)):

$$E_{th} = E_{th}^{0} + (R\ T/\ n\ F)\ \ln(P_{H2}\ (P_{O2})^{1/2})\ , \quad (2)$$

where:

E_{th}^{0}: theoretical voltage calculated at standard operating conditions (at 25 °C and 1 bar),

F: Faraday constant (= 96485 [C mol^{-1}]),

n: number of electrons involved in the reaction,

p_{H2}: partial pressure of hydrogen, bar,

p_{O2}: partial pressureof oxygen, bar,

R: universal gas constant (= 8,314 [J K^{-1} mol^{-1}]),

T: operating temperature, °K.

Ohmic losses are linked to the transport of electrical charges in the membrane (proton transport) and in the electrodes (electron transport) as well as to the losses at contact surfaces of the different layers (for example between the active and diffusion layers). They also take into account the ohmic losses of the electrical circuit up to the various points of voltage measurement. The voltage drop related to ohmic losses is proportional to the current I according to Ohm's law:

$$\eta_{ohm} = R_{ohm}\ I \quad (3)$$

In this study, R_{ohm} is directly measured by EIS at high-frequency, this connection is supposed to be the first link between the polarization curve identification and EIS.

For the activation losses, as shown in Equation (4), their formula is calculated using Tafel assumption [33]:

$$\eta_{act} = (R.T)/\ (\alpha.n.F)\ \ln((I+I_n)/I_0), \quad (4)$$

where I_0 is the activation current, I_n the crossover current, image of the internal gas permeation and α the charge transfer coefficient. This coefficient is assumed constant (equal to 0.5) and invariant as a function of operating conditions according to various bibliographic references [34] [35].

As for diffusion losses, the evolution of gases concentration can be described by Fick's law, the resolution of this law in stationary, as described in [36], allows to estimate the voltage drop due to diffusion losses as shown in Equation (5):

$$\eta_{diff} = - (R.T)/ (\beta.n.F) \ln(1 - I/ I_{lim}), \quad (5)$$

β is a coefficient taking into account the complexity of the porous layers constituting the electrodes, it can also be linked to the order of reaction [20], its value is identified experimentally. I_{lim} is the limit current, corresponding to the maximum theoretical current that could be supplied by the FC.

It is to note that the closer the current value to the limit current I_{lim}, the less the system becomes able to maintain the necessary concentration of gases, leading subsequently to a voltage drop of the component.

The identification of the QS model is carried out for each V-I curve to make it possible to assess the evolution of each loss over time. The vector θ of the global identification problem is shown in Equation (6).

$$\theta = [I_n ; I_0 ; \beta ; I_{lim}] \quad (6)$$

The proposed approach is therefore to follow the temporal evolution of this vector throughout the ageing campaign in order to analyze the evolution of the SoH of the fuel cell stack.

Given the non-linear nature of the model, the Matlab optimization function (lsqnonlin) makes it possible to establish the identification algorithm dedicated to fit experimental data. This function makes use of an algorithm called Trust-Region-Reflective Least Squares [37] [38]. It is a deterministic algorithm which evolution does not depend on random events. I.e., for the same starting point, the algorithm will always give the same result. In addition to its ability to deal with non-linear problems, this algorithm is able to handle domain constraints. This point interests us particularly in the context of our identification problem, since the parameters constituting our vector of parameters are subject to boundary constraints, particularly constraints preventing them to be negative.

We also note that the used algorithm can be described as a local algorithm. Unlike a global algorithm, a local algorithm may not converge to the global minimum of a function but to a local minimum. Its ability to find the global minimum depends essentially on the initial point or starting point of the algorithm. Hence the need of a study of parameters dispersion after each identification process.

2.2. Experimental procedure

2.2.1. Ageing campaigns presentation

The objective of these campaigns is to obtain three different levels of severities in terms of degradation using different power profiles at constant operational conditions (T= 65 °C, gases pressures P_{H2} = 1.5 bar / P_{Air}= 1.5 bar, relative humidities of gases RH_{H2}= 50 % / RH_{Air}= 50 %, stoichiometries λ_{H2}= 1.5 / λ_{Air}= 2). The profiles of the three campaigns (Mission profile, P_{min} and P_{max}) are shown in **Fig. 2**. A summary of cumulative hours and number of characterizations of each profile is given in Table 1.

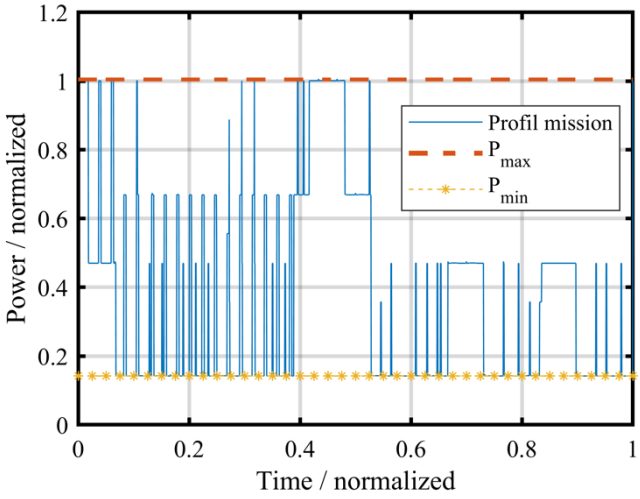

Fig. 2. Profiles of the 3 ageing campaigns (Mission profile, P_{min} and P_{max})

Table 1. Summary of cumulative hours and the number of characterizations of each ageing campaign

	Ageing campaign 1 'Mission profile'	**Ageing campaign 2 'Pmin'**	**Ageing campaign 3 'Pmax'**
Cumulative hours [h]	1,100	914	894
Number of characterization phases	13	10	8

2.2.2. Experimental data

In this study, we will think in terms of equivalent average cell voltage. This voltage is equal to the stack voltage divided by the number of cells assuming that the voltages of cells are well balanced. Given the repetitive character of the process for the 3 campaigns, we will only propose here details for the first campaign whose polarization curves are shown in Fig. **3**(a).

For this campaign, two singular characterizations are to be reported (characterizations 5 and 6). These characterizations were performed after a nitrogen inerting at operating temperature of the stack due to an emergency stop

(auxiliaries' failure). The stack has dried up causing a drop in performance. Except for these two characterizations, we clearly note a decrease in stack performance over time (corresponding to 48 µV h^{-1} at 1 A cm^{-2}) between the first (characterization 1 - 0 h) and last characterization (characterization 13 - 1101 h) of Fig. **3**(a).

For three current densities (0.08 A cm^{-2}, 0.55 A cm^{-2} and 1 A cm^{-2}), Fig. **3**(b) shows the calculation of the ratio between the voltages for each characterization with respect to the voltage of the first characterization. It clearly appears that the voltage degradation increases with the considered current of the V-I curves.

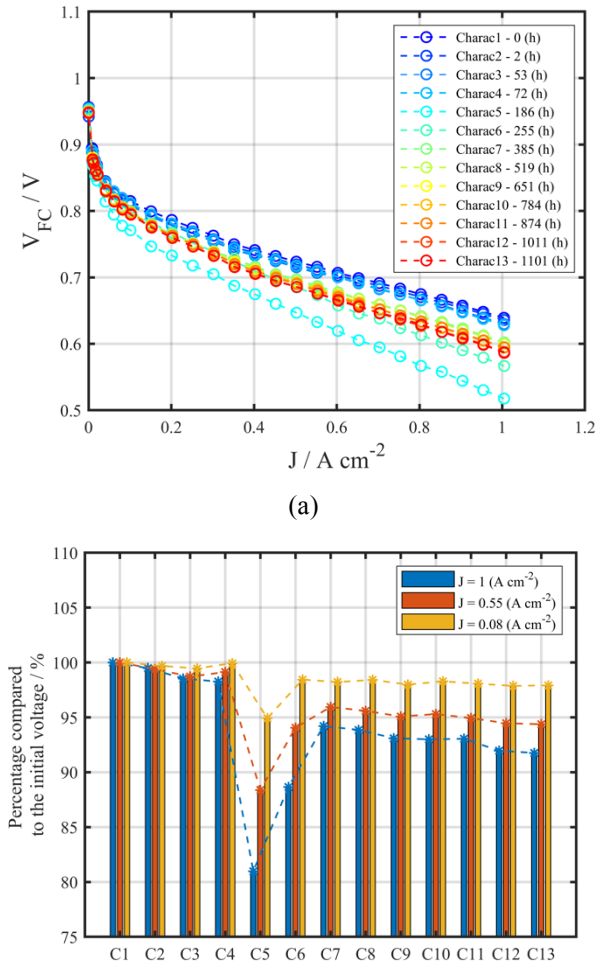

C1: Charac 1 – 0 (h)
C2: Charac 2 – 2 (h)
C3: Charac 3 – 53 (h)
C4: Charac 4 – 72 (h)
C5: Charac 5 – 186 (h)
C6: Charac 6 – 255 (h)
C7: Charac 7 – 385 (h)
C8: Charac 8 – 519 (h)
C9: Charac 9 – 651 (h)
C10: Charac 10 – 784 (h)
C11: Charac 11 – 874 (h)
C12: Charac 12 – 1011 (h)
C13: Charac 13 – 1101 (h)

Fig. 3. (a) Experimental V-I curves and (b) Evolution of the degradation rates for three currents for campaign 1 'Mission profile' (equivalent average cell) at T = 65 °C, P_{H2} = 1.5 bar/ P_{Air} = 1.5 bar, RH_{H2} = 50 % / RH_{Air} = 50 % and λ_{H2} = 1.5 / λ_{Air} = 2.

As mentioned before, a measurement of R_{ohm} coming from EIS data at high-frequency is necessary to separate the different losses from the polarization curves. An example of EIS data is shown in Fig. **4** for all characterizations of campaign 1 at 1 A cm^{-2}. Extracted values of R_{ohm} are also represented as a function of current for each characterization of the campaign 1 in Fig. **4**.

It is noted that the high values of the ohmic resistance of the stack R_{ohm} for the characterizations 5 and 6 are justified by the drying caused by a nitrogen inerting after an emergency stop, mentioned previously.

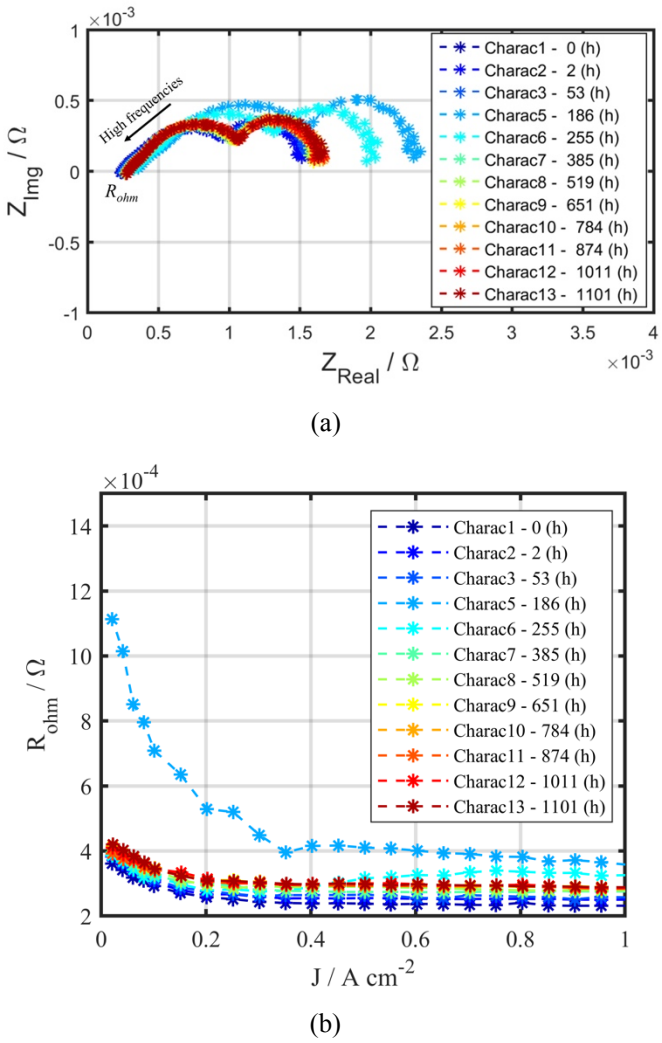

Fig. 4. (a) EIS data at 1 A cm^{-2} for all characterizations of campaign 1 and (b) R_{ohm} measured *via* EIS data at high-frequency as a function of current for each characterization of campaign 1 (T = 65 °C, P_{H2} = 1.5 bar/ P_{Air} = 1.5 bar, RH_{H2} = 50 %/ RH_{Air} = 50 %, λ_{H2} = 1.5/ λ_{Air} = 2).

3. Results and discussions

3.1. Experimental data fitting

After the identification of V-I curves, we calculate the relative error between experimental and model fitting data. The corresponding maximum relative error of each characterization is given in Fig. **5**. We note a very good correspondence between experimental and model data with a maximum error of less than 1 %. The reproducibility of these results has been tested by multiple identifications with randomly initialized starting points.

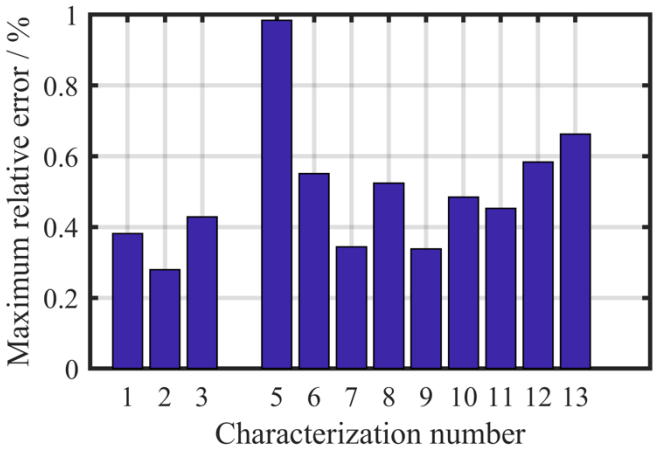

Fig. 5. Maximum relative error between experimental data and model fitting

It should be noted that the noisy data of characterization number 4 prevents the good determination of R_{ohm}, thus not allowing the identification of the V-I curve of this characterization.

3.2. Losses separation and their temporal tracking

Besides the quality of experimental data fitting, the model allows losses separation and their tracking over time. Fig. **6** shows the evolution of ohmic, diffusion and activation losses as a function of the number of each characterization of campaign 1.

The activation losses are dominant. At 1 A cm^{-2}, the activation losses represent 79 % of the total losses of the characterization 1 whereas the diffusion losses represent only 14 % and the ohmic losses 8 % of the total losses. Several studies support this finding, they have shown that activation losses remain predominant compared to other losses [15].

Except for the characterizations 5 and 6, the losses increase almost linearly over time as shown in Fig. **7**. The biggest increase in losses is that of the diffusion losses. In fact, these losses increase by 36 % between characterization 1 and 13 at 1 A cm^{-2}, followed by the ohmic losses increasing by 25 %. The activation losses only increase by 3 % of their initial value.

Concerning the characterizations 5 and 6, we can conclude that the drying has affected all the phenomena, and not only the membranes. This drying has in fact also degraded temporarily the active layer/ membrane interfaces limiting the transport of protons and therefore the effective active area, generating respectively an increase in diffusion and activation losses. The same conclusions have been reached by applying the approach to data concerning a single cell as presented in [15].

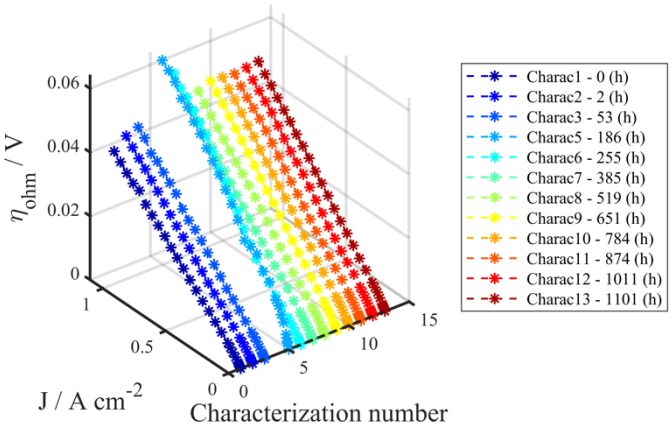

(a)

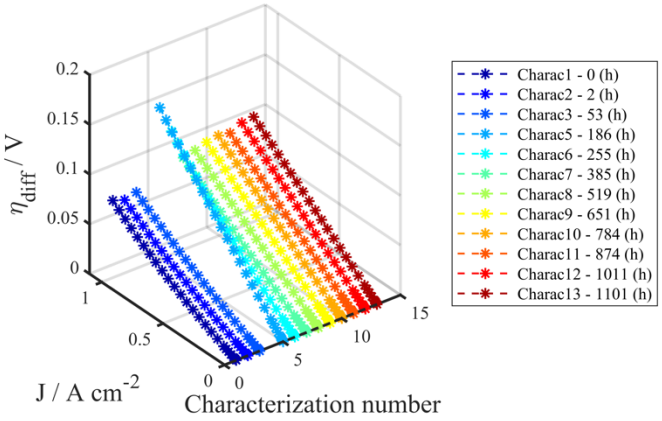

(b)

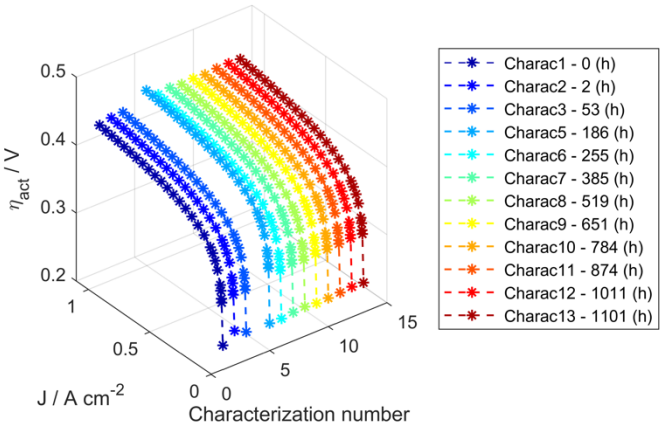

(c)

Fig. 6. Losses separation of each characterization of campaign 1 for an average equivalent cell : (a) Ohmic, (b) diffusion and (c) activation losses (T = 65 °C, P_{H2} = 1.5 bar/ P_{Air}= 1.5 bar, RH_{H2}= 50 %/ RH_{Air}= 50 %, λ_{H2}= 1.5/ λ_{Air}= 2).

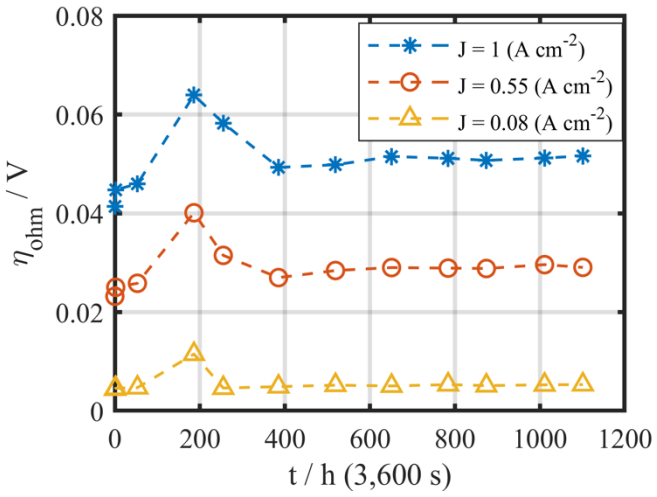

(a)

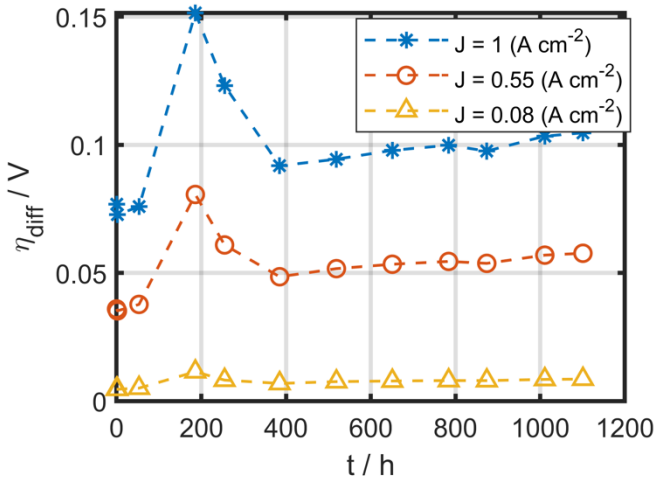

(b)

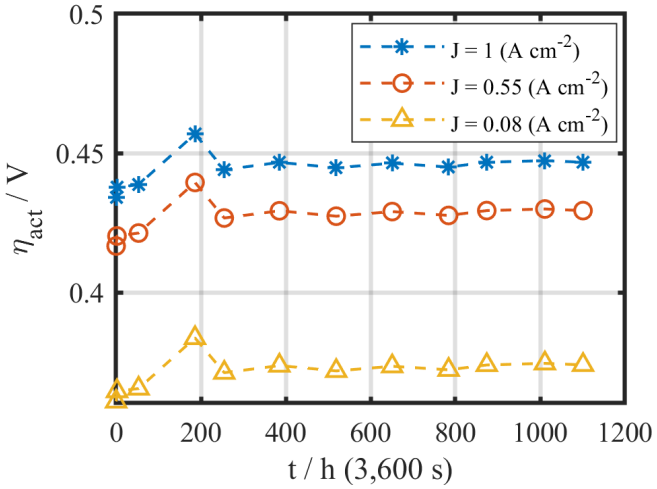

(c)

Fig. 7. (a) Ohmic, (b) diffusion and (c) activation losses evolution over time of campaign 1 for 1, 0.55 and 0.08 A cm^{-2} at T = 65 °C, P_{H2} = 1.5 bar/ P_{Air}= 1.5 bar, RH_{H2}= 50 %/ RH_{Air}= 50 % and λ_{H2}= 1.5/ λ_{Air}= 2.

3.3. Monitoring of model parameters

In this part, we compare, firstly, the evolution of the values of parameter I_0 (obtained *via* the model identification) with the values of the ElectroChemical active Surface Area (ECSA) calculated by Cyclic Voltammetry (CV) [36] [39] at the same operational conditions with a voltage scan rate of 100 mV s^{-1} from 50 mV to 850 mV. The ECSA (in cm_{pt}^2 cm^{-2}) is assimilated to the real used surface of platinum. It is the image of the current corresponding to the peak of the anodic scanning issued from voltammetry [31]. An example of this comparison for the first campaign 'mission profile' for some characterizations where the VC was performed is shown in Fig. **8** as a function of time.

Secondly, as the cyclic voltammetry leads also to estimate the equivalent current for the H_2 crossover (whose parameter I_n is supposed here to be an image) [10] [31], a comparison between the values of this parameter obtained by model identification and CV is done in Fig. **8** for the first ageing campaign.

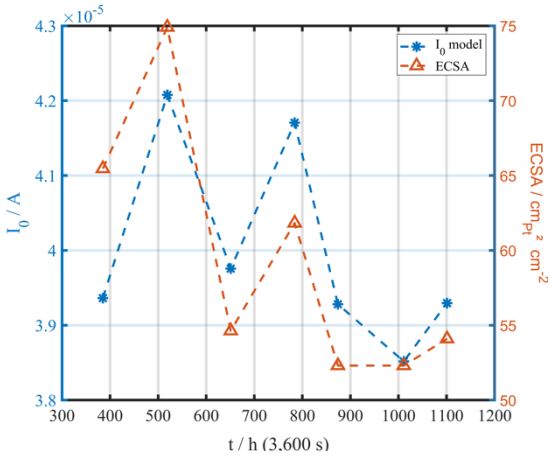

(a)

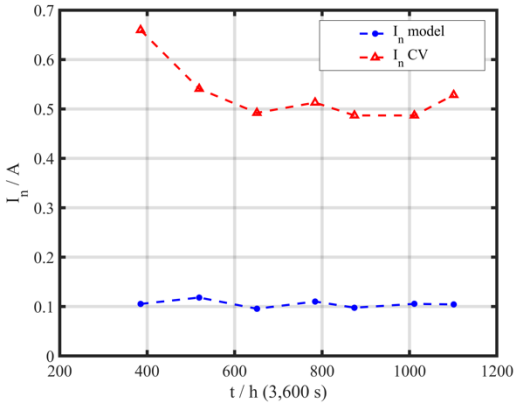

(b)

Fig. 8. Comparison between parameter obtained *via* the model identification and those obtained *via* CV for the first ageing campaign: (a) ECSA and I_0 as a function of time; (b) I_n obtained by model identification *vs* I_n obtained by CV

As obtained in our previous work concerning a single cell [15], the parameter I_0 is a good image of the ECSA. In Fig. **9**,

we plot the ECSA as a function of the activation current I_0 for the 3 ageing campaigns. It may be noted that a good correlation can be reached between these two parameters.

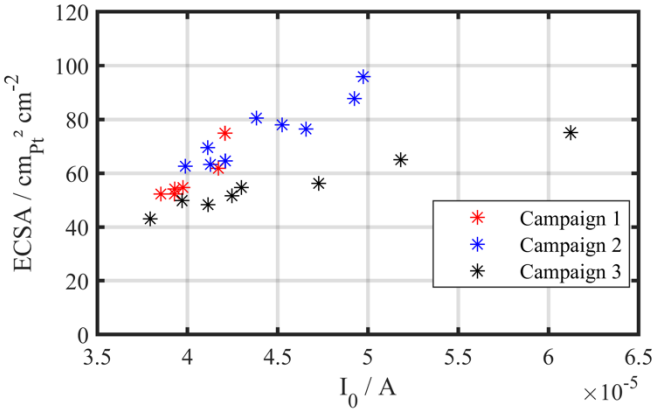

Fig. 9. Evolution of the ECSA as a function of I_0 for the 3 ageing campaigns

We can observe a clear linearity between I_0 and ECSA. If the linearity coefficients are close for the campaigns 1 and 2, it is not the case for the campaign 3. That could be a consequence of differences between stacks (platinum dispersion, stack clamping, break-in of the stack…).

Contrarily to the results obtained in the case of a single cell [15], the parameter I_n obtained by modelling is rather different from the crossover current obtained by CV (classically the reference value). A ratio of 5 to 6 can be observed between both values. So far, these differences are not really understood. The number of points at low current range densities could be an explanation, the value of I_n being very sensitive to this factor. A good understanding of the difference between CV of a stack and CV of a cell could provide more explanations leading afterward to a FC prognostic [40].

4. Conclusion

In this article, an identification process fed by V-I curve and EIS data (used in this study to estimate R_{ohm}) was introduced allowing to identify parameters of a QS model describing the phenomena involved in the FC. The proposed model was built through specific physicochemical laws, such as activation and diffusion.

Thanks to the QS model and by assuming that the charge transfer coefficient α is equal to 0.5, the presented study makes it possible to assess the FC performances and to track its voltage drops over time. In that context, three ageing campaigns have been tested and compared to demonstrate that the proposed approach got sensitiveness to degradations over time.

The first achieved results are encouraging for a SoH assessment. In addition to the voltage drops tracking, the follow-up of the SoH of the Active Layer (AL) can be carried out through the evolution of the activation current I_0. Indeed, we can conclude that the identified values for I_0 have the same evolution as the reference values measured by CV.

Although the V-I curve could provide a global overview in the QS mode, it does not give a dynamic view of the FC performances. So far, EIS was only used for the ohmic resistance estimation. A deeper exploitation of EIS will be presented in another article.

Identification of EIS data was indeed done *via* a 'without *a priori*' approach concerning a single cell FC in our previous studies. First results confirm the potentiality of this approach; they proved that such a perspective can offer further information to investigate the monitoring of the SoH and the ageing of a FC stack.

Another perspective of this work consists to adapt the developed methodology for an online diagnosis. For this purpose, different improvements must be performed to enhance the protocol of measurements (number and durations) and characterization phases (start and stop phases for instance).

Acknowledgements

The presented work in this article is a part of FUCHYA project led by the Institut de Recherche Technologique IRT Saint-Exupéry, Agence Nationale de la Recherche ANR, Safran, Airbus and the Laplace laboratory. Authors would like to present their thanks to all the project partners.

References

[1] M. Inaba, T. Kinumoto, M. Kiriake, R. Umebayashi, A. Tasaka, and Z. Ogumi, 'Gas crossover and membrane degradation in polymer electrolyte fuel cells', Electrochimica Acta, vol. 51, no. 26, pp. 5746–5753, August 2006. (Article)

[2] F. A. de Bruijn, V. A. T. Dam, and G. J. M. Janssen, 'Review: Durability and Degradation Issues of PEM Fuel Cell Components', Fuel Cells, vol. 8, no. 1, pp. 3–22, February 2008. (Article)

[3] R. L. Borup, J. R. Davey, F. H. Garzon, D. L. Wood, and M. A. Inbody, 'PEM fuel cell electrocatalyst durability measurements', Journal of Power Sources, vol. 163, no. 1, pp. 76–81, December 2006. (Article)

[4] Joseph W. Pratt, Leonard E. Klebanoff, Karina Munoz-Ramos, Abbas A. Akhil, Dita B. Curgus, and Benjamin L. Schenkman, 'Proton Exchange Membrane Fuel Cells for Electrical Power Generation On-Board Commercial Airplanes'. January 2013. (Article)

[5] A. K. Sehra and W. Whitlow, 'Propulsion and power for 21st century aviation', Progress in Aerospace Sciences, vol. 40, pp. 199–235, May 2004. (Article)

[6] US Drive, 'Fuel Cell Technical Team Roadmap'. Driving research and innovation for vehicle efficiency and energy sustainability, November 2017. (Standards and Reports)

[7] B. Mebarki, B. Allaoua, B. Draoui, and D. Belatrache, 'Study of the energy performance of a PEM fuel cell vehicle', International Journal of Renewable Energy Research (IJRER), vol. 7, no. 3, Art. no. 3, September 2017. (Article)

[8] T. Azib, G. Remy, O. Bethoux, C. Marchand, 'Control strategy with saturation management of a fuel cell/ultracapacitors hybrid vehicule' 2010 IEEE Vehicle Power and Propulsion Conference, September 2020. (Article)

[9] C. Nevoloso, N. Campagna, M. Caruso, V. Castiglia, A. O. D. Tommaso, and R. Miceli, 'Interior Permanent Magnet Synchronous Machine Drive Powered by Fuel Cell for Automotive Applications', in 2020 9th International Conference on Renewable Energy Research and Application (ICRERA), pp. 499–504, September 2020. (Article)

[10] T. Génevé, C. Turpin, J. Régnier, O. Rallières, O. Verdu, A. Rakotondrainibe and K. Lombard, 'Voltammetric Methods for Hydrogen Crossover Diagnosis in a PEMFC Stack', Fuel Cells, vol. 17, no. 2, pp. 210–216, April 2017. (Article)

[11] G. De Moor, C. Bas, N. Charvin, E. Moukheiber, F. Niepceron, N. Breilly, J. André, E. Rossinot, E. Claude, N. D. Albérola and L. Flandin, 'Understanding membrane failure in PEMFC: comparison of diagnostic tools at different observation scales', Wiley, vol. 12, no. 3, pp. 356–364, March 2012. (Article)

[12] S. Jemeï 'Diagnostics and Prognostics of Fuel Cell Generators', in Hybridization, Diagnostic and Prognostic of Proton Exchange Membrane Fuel Cells, John Wiley & Sons, Ltd, pp. 115–185, Octobre 2018. (Book Chapter)

[13] R. Petrone, D. Hissel, M. C. Péra, D. Chamagne, and R. Gouriveau, 'Accelerated stress test procedures for PEM fuel cells under actual load constraints: State-of-art and proposals', International Journal of Hydrogen Energy, vol. 40, no. 36, pp. 12489–12505, September 2015. (Article)

[14] Z. Zheng, R. Petrone, MC. Pera, D. Hissel, M. Béchérif, C. Pianese, NY. Steiner, M. Sorrentino 'A review on non-model based diagnosis methodologies for PEM fuel cell stacks and systems', International Journal of Hydrogen Energy, vol. 38, no. 21, pp. 8914–8926, July 2013. (Article)

[15] S. El Aabid, J. Regnier, C. Turpin, O. Rallières, E. Soyez, N. Chadourne, J. D'Arbigny, T. Horde, E. Foch, 'A global approach for a consistent identification of static and dynamic phenomena in a PEM Fuel Cell', Mathematics and Computers in Simulation, October 2018. (Article)

[16] T. Génevé, J. Régnier, and C. Turpin, 'Fuel cell flooding diagnosis based on time-constant spectrum analysis', International Journal of Hydrogen Energy, vol. 41, no. 1, pp. 516–523, January 2016. (Article)

[17] A. Rubio and W. Agila, 'Dynamic Model of Proton Exchange Membrane Fuel Cells: A Critical Review and a Novel Model', in 2019 8th International Conference on Renewable Energy Research and Applications (ICRERA), pp. 353–358, November 2019. (Article)

[18] X. Yan, M. Hou, L. Sun, D. Liang, Q. Shen; H. Xu, P. Ming, B. Yi, 'AC impedance characteristics of a 2kW PEM fuel cell stack under different operating conditions and load changes', International Journal of Hydrogen Energy, vol. 32, no. 17, pp. 4358–4364, December 2007. (Article)

[19] A. Pessot, C. Turpin, A. Jaafar, E. Soyer, O. Rallières. G. Gager, J. D'Arbigny, 'Contribution to the modelling of a low temperature pem fuel cell in aeronautical conditions by design of experiments', Mathematics and Computers in Simulation, August 2018. (Article)

[20] I. Labach, O. Rallières, and C. Turpin, 'Steady-state Semi-empirical Model of a Single Proton Exchange Membrane Fuel Cell (PEMFC) at Varying Operating Conditions', Fuel Cells, vol. 17, no. 2, pp. 166–177, April 2017. (Article)

[21] Y. Tsuchiya, Y. Hayashi, Y. Fujimoto, A. Yoshida, and Y. Amano, 'Hot Water Demand Prediction Method for Operational Planning of Residential Fuel Cell System', in 2019 7th International Conference on Smart Grid (icSmartGrid), pp. 46–51, December 2019. (Article)

[22] N. Fouquet, C. Doulet, C. Nouillant, G. Dauphin-Tanguy, and B. Ould-Bouamama, 'Model based PEM fuel cell state-of-health monitoring via ac impedance measurements', Journal of Power Sources, vol. 159, no. 2, pp. 905–913, September 2006. (Article)

[23] J.-M. Le Canut, R. M. Abouatallah, and D. A. Harrington, 'Detection of Membrane Drying, Fuel Cell Flooding, and Anode Catalyst Poisoning on PEMFC Stacks by Electrochemical Impedance Spectroscopy', Journal of The Electrochemical Society, vol. 153, no. 5, p. A857, 2006. (Article)

[24] C. Restrepo, T. Konjedic, J. Calvente, and R. Giral, 'A Review of the Main Power Electronics' Advances in Order to Ensure Efficient Operation and Durability of PEMFCs', Automatika, vol. 53, no. 2, pp. 184–198, January 2012. (Article)

[25] A. Rubio, W. Agila, L. Miranda, and B. Lima, 'Real-Time Qualitative Model for Estimate Water Content in PEM Fuel Cell', in 2019 8th International Conference on Renewable Energy Research and Applications (ICRERA), pp. 455–459, November 2019. (Article)

[26] E. Cho, 'A Study on Performance Degradation of PEMFC by Water Freezing', J. Electrochem. Soc, vol. 150, no. 12, pp. A1667–A1670, 2003. (Article)

[27] W. Mérida, D. A. Harrington, J. M. Le Canut, and G. McLean, 'Characterisation of proton exchange membrane fuel cell (PEMFC) failures via electrochemical impedance spectroscopy', Journal of Power Sources, vol. 161, no. 1, pp. 264–274, October 2006. (Article)

[28] G. Mousa, J. DeVaal, and F. Golnaraghi, 'Diagnosis of hydrogen crossover and emission in proton exchange membrane fuel cells', International Journal of Hydrogen Energy, vol. 39, no. 36, pp. 21154–21164, December 2014. (Article)

[29] G. Mousa, F. Golnaraghi, J. DeVaal, and A. Young, 'Detecting proton exchange membrane fuel cell hydrogen

leak using electrochemical impedance spectroscopy method', Journal of Power Sources, vol. 246, pp. 110–116, January 2014. (Article)

[30] M. Perez Page and V. Pérez-Herranz, 'Study of the electrochemical behaviour of a 300 W PEM fuel cell stack by Electrochemical Impedance Spectroscopy', International Journal of Hydrogen Energy, vol. 39, pp. 4009–4015, March 2014. (Article)

[31] T. Génevé, 'Méthodes de diagnostic des piles à combustible', Thèse doctorale, Institut National Polytechnique de Toulouse INPT, 2016. (PhD thesis)

[32] X. Yuan, H. Wang, J. Colin Sun, and J. Zhang, 'AC impedance technique in PEM fuel cell diagnosis - A review', International Journal of Hydrogen Energy, vol. 32, no. 17, pp. 4365–4380, December 2007. (Article)

[33] G. Fontes, C. Turpin, S. Astier, and T. A. Meynard, 'Interactions Between Fuel Cells and Power Converters: Influence of Current Harmonics on a Fuel Cell Stack', IEEE Transactions on Power Electronics, vol. 22, no. 2, pp. 670–678, March 2007. (Article)

[34] M. Aghighi, M. A. Hoeh, W. Lehnert, G. Merle, and J. Gostick, 'Simulation of a full fuel cell membrane electrode assembly using pore network modeling', Journal of The Electrochemical Society, vol. 163, no. 5, pp. F384–F392, 2016. (Article)

[35] K. C. Neyerlin, W. Gu, J. Jorne, and H. A. Gasteiger, 'Determination of Catalyst Unique Parameters for the Oxygen Reduction Reaction in a PEMFC', Journal of The Electrochemical Society, vol. 153, no. 10, p. A1955, 2006. (Article)

[36] G. Fontès, 'Modélisation et caractérisation de la pile PEM pour l'étude des interactions avec les convertisseurs statiques', Thèse doctorale, Institut National Polytechnique de Toulouse INPT, 2005. (PhD thesis)

[37] A. R. Conn, K. Scheinberg, and L. N. Vicente, Introduction to derivative-free optimization. Philadelphia Society for Industrial and Applied Mathematics, 2008. (Article)

[38] T. M. Le, B. Fatahi, H. Khabbaz, and W. Sun, 'Numerical optimization applying trust-region reflective least squares algorithm with constraints to optimize the non-linear creep parameters of soft soil', Applied Mathematical Modelling, vol. 41, pp. 236–256, January 2017. (Article)

[39] E. Brightman, G. Hinds, and R. O'Malley, 'In situ measurement of active catalyst surface area in fuel cell stacks', Journal of Power Sources, vol. 242, pp. 244–254, November 2013. (Article)

[40] K. CHEN, S. Laghrouche, and A. Djerdir, 'Proton Exchange Membrane Fuel Cell Degradation and Remaining Useful Life Prediction based on Artificial Neural Network', in 2018 7th International Conference on Renewable Energy Research and Applications (ICRERA), pp. 407–411, October 2018. (Article)